ELSEVIER

# Confocal Raman and TEM measurements at the same area on nanoparticles

M. Cazayous [a,b,*], C. Langlois [a,b], T. Oikawa [a,c], C. Ricolleau [a,b], A. Sacuto [a,b]

[a] *Laboratoire Matériaux et Phénomènes Quantiques (UMR 7162), Université Denis-Diderot (Paris 7), 2 place Jussieu, 75251 Paris, France*
[b] *Laboratoire de Physique des Solides (UPR5 CNRS), Ecole Supérieure de Physique et de Chimie Industrielle, 10 rue Vauquelin, 75231 Paris, France*
[c] *Application and Research Center, JEOL Ltd., 3-1-2 Musashino, Akishima, Tokyo 196-8558, Japan*

Available online 17 November 2006

## Abstract

We have studied Cu–Ag core-shell nanoparticles using a confocal Raman setup reducing the number of probed nanoparticles from $10^8$ for a macroscale to $10^3$–$10^4$. This advance represents a significant step towards resolving the signature of a single particle. Cu–Ag core-shell and pure Ag nanoparticles have been identified on the same spectra. The size and form of these nanoparticles deduced from Raman spectra are in agreement with the ones measured by transmission electron microscopy (TEM). The intensity of the micro-Raman signal has been correlated with the exact distribution of nanoparticles obtained by TEM on the same area. Two Raman signatures depending on the acoustic mismatch between Cu core and Ag shell have been pointed out and correlated to the different orientations of their crystallographic axis.
© 2006 Elsevier B.V. All rights reserved.

*Keywords:* Raman; Nonoparticles; Electron microscopy

## 1. Introduction

Metallic nanoparticles are currently attracting most interest for their properties resulting from the confinement of electrons and phonons. The surface-enhanced Raman scattering (SERS) used the excitation of the confined electrons to generate intense local fields and to greatly enhance sensitivity in the spectroscopic signal of molecules absorbed onto the nanoparticles [1,2]. A layered nanoparticles with a dielectric core and a metallic shell, known as core-shell nanoparticle, provides a tunable geometry to control the magnitude of the local field. Understanding SERS based on the light/plasmon interaction in metallic nanoparticles is still a challenge. In particular, the role played in this process by acoustic phonons confined in the core-shell nanoparticles has to be clarified [3]. For an isolated spherical particle, the phonon density of state is discrete and the confined vibrations are expressed into torsional and spheroidal modes. The spheroidal modes have a mixed character of radial and tangential motions. Many experimental works showed that the quadripolar vibrations corresponding to spheroidal vibrations with two deformation axes strongly come out in the Raman spectra. The pure radial modes known as breathing modes appear only in systems with narrow size distributions [4]. The study of the vibration modes has to be coupled with the local investigation of the structural properties of the nanoparticles in order to tame the SERS effect. The vibrational frequencies of acoustic modes in nanoparticles are in the Raman detectable range making this experimental technique an invaluable tool for studying these vibration modes [5–7]. Up to now, Raman scattering on nanoparticles has been limited to macroscopic scale avoiding the link between the local structural and vibrational properties.

In this work, we investigate Cu–Ag core shell nanoparticles comparing micro Raman and transmission electron microscopy (TEM) measurements. The confocal Raman setup reduces the probed size to 0.7 μm and the number of probed nanoparticles from $10^8$ to $10^3$–$10^4$. On the same sample, the Raman signature of Cu–Ag core-shell and pure

Ag nanoparticles have been identified. Several TEM techniques have been used to determine the structural properties of the nanoparticles on the same area probed by Raman. The size, form and composition of these nanoparticles deduced from Raman spectra are in agreement with the ones measured by TEM. The intensity of the micro-Raman spectra allows to extract the same distribution of nanoparticles obtained by TEM. Two Raman signatures depending on the acoustic mismatch between Cu core and Ag shell have been pointed out. A correlation to the different orientations of their crystallographic axes has been established.

## 2. Sample production and characterization

Nanoparticles are elaborated from successive thermal evaporation of Cu and Ag under ultra-high vacuum conditions directly onto a thin amorphous carbon film and supported by a microscopy grid with micro-numerated square holes. Typically, evaporation rates for Cu and Ag were around 0.25 nm/min. Pressure inside the deposition room was below $10^{-7}$ Torr. The substrate is heated at a temperature of 400 °C. After this operation, the nanoparticles are annealed during half an hour at the same temperature. Sample A contains Cu nanoparticles obtained by 2 nm Cu deposition covered by a 1.5 nm aluminium layer deposited by plasma laser deposition in order to avoid the oxidization of the Cu particles. Sample B has been elaborated with the same Cu deposition as sample A followed by 1 nm of Ag without any additional aluminium film. Several TEM techniques were used to characterize sample A and B: High Resolution imaging (HRTEM), energy filtered imaging (EFTEM) and scanning high angle dark field imaging (HAADF-STEM) [8,9]. The microscope used for this study was a JEOL 2100 working at 200 keV with an HAADF detector and a Gatan energy filter mounted on the microscope column. Energy filtered imaging consists in spreading the electron beam with a magnetic prism after the sample in order to reconstruct images only with electrons that have lost a specific part of their energy by inelastic interactions with the different elements present in the sample. In our case, this technique was used to obtain a chemical map of Ag, emphasizing the core-shell structure. HAADF experiments were used to obtain images of the sample with strong black and white contrast, allowing intensity thresholding and particle shape recognition for a statistical study of the size and morphology of the particles.

The Raman scattering spectra were recorded at room temperature using triple spectrometer Jobin Yvon T 64,000 with a high rejection rate in order to measure the low frequency Raman signal closed to the Rayleigh scattering. We used several excitation lines from a $Ar^+$– $Kr^+$ mixed gas laser. The laser beam was guided into a microscope and focused through a ×50 long working distance objective with a numerical aperture of 0.4. The scattered light was collected by the same objective. The samples were kept in vacuum in order to avoid Raman

lines arising from air molecules at low frequencies and tilted at 40° from the incident light direction to reject its reflection out of the objective. The initial spot diameter was about 1.5 μm and was reduced to 0.7 μm by the confocal setup. A better spot size cannot be achieved due to the tilt angle of the samples. The number of particles analyzed under the Raman spot is of the order of $10^3$–$10^4$ as deduced from the nanoparticule density of $10^4$ μm$^{-2}$ measured by TEM. This value has to be compared to macroscopic values closed to $10^8$ contained within a standard spot diameter of 100 μm. The Raman and TEM measurements have been performed on the same area. The area of interest was the channel formed by the letter R of the numeration items and the rods of the microscopy grid (see inset in Fig. 2a). Therefore, Raman spectra are directly correlated with the exact nanoparticule distribution obtained by TEM on the same area.

## 3. Model

The Raman peaks associated with the vibration modes of nanoparticles come from a modulation of surface polarization charges via a deformation potential mechanism [10,11]. The modulation is due to a modification of the nanoparticle surface orientation during the nanoparticle oscillation. A complete description of the Raman peak, in particular the intensity ratios between the different torsional and spheroidal modes, need to take into account the various coupling mechanisms between the surface plasmon–polaritons and the confined vibrations. Here, we limit our interest to the vibrational properties classically basely described by Lamb theory [12]. This latter demonstrates that the Raman shift $\omega$ of an elastic sphere with a free surface are inversely proportional to the diameter $D$ of nanoparticle and proportional to the transversal sound velocity $v_t$ ($c$ being the vacuum light speed),

$$\omega = \frac{v_t}{cD}S. \tag{1}$$

Factor $S$ depends on the mode and on the ratio of the transversal and longitudinal sound velocities. The $S$ factor is close to 0.85 for the both fundamental quadrupolar modes of Ag and Cu. The transversal sound velocities are $v_t = 2300$ m/s and $v_t = 1660$ m/s for Cu and Ag, respectively. From Eq. (1), the frequency of the Raman low frequency peak allowed to calculate the nanoparticle diameter that has to be compared to the maximum of the size distribution measured by TEM.

For core-shell nanoparticles, the frequency of the quadrupolar modes can be calculated with the Lamb approach including the resolution of the Navier equation using the continuous medium approximation [13]. We assume the continuity of both the vibrational displacement and the force at the core/shell interface and no force at the shell/ air interface. We have an internal total reflection of the acoustic waves at the shell–air interface: the sphere is considered as free.

## 4. Experiments and simulations

Fig. 1a shows the Stokes–antiStokes Raman spectra recorded at low frequencies on Cu nanoparticles in the R channel (Fig. 2). Only one spectrum is presented for each wavelength since no changes have been observed for sample A along the channel. The observed peak clearly not related to the Rayleigh line (centered at $0 \, cm^{-1}$) is associated with the fundamental mode of the quadripolar vibrations [5–7]. The diameter $D$ of the Cu nanoparticles is calculated from Eq. (1) using the frequency at the maximum intensity of the low frequency peak recorded at 2.7 eV. As it can be seen in Table 1, the diameter obtained from Raman is in agreement with the one measured by TEM. Fig. 2a and b shows the bright field TEM image of Cu nanoparticles and the associated diameter distribution used to the comparison with Raman measurements.

In Fig. 1a The Stokes peak shifts from $7.2 \, cm^{-1}$ to $6.5 \, cm^{-1}$ when the energy of the incident light decreased from 2.7 eV to 1.65 eV. The Raman scattering is observed when the light excites the dipolar surface plasmon. This means that an effect of resonance occurs. To interpret the frequency shift of the quadripolar mode with the incident wavelength, the morphology of the nanoparticle has to be considered. If the nanoparticle is ellipsoidally distorted and has a prolate shape, the degenerate dipolar plasmon is splitted for giving a lower energy nondegenerate plasmon which corresponds to a dipole oscillating along the large axis and a higher energy plasmon with a dipole oscillating in the plane perpendicular to this large axis [7]. It has been shown that the atoms moving along the large axis are coupled to the plasmon with the lower energy precisely excited in the red. The red shift involves nanoparticles with an ellipsoidal shape due to the tuning of the plasmon resonance. Our TEM measurements show the ellipsoidal shape of the Cu nanoparticles with mean minor and major axes diameter of 8.3 and 11.5 nm. In the approximation of a sphere shape, the diameter deduced from Raman spectra is 10.5, 11.2 and 12 nm for 2.7, 2.41 and 1.65 eV excitation energies, respectively. The mean nanoparticle diameters measured with the three excitation lines correspond closely to the value of the mean major axis obtained by TEM. This selection based on the shape of the nanoparticles allowed to reduce the number of nanoparticles probed. For the nanoparticles with a mean diameter of 10.5 nm selected at 2.7 eV, the number of observed nanoparticles can be estimated at 40% of the total distribution determined by TEM under the laser spot.

Notice that the absolute scales of Raman spectra displayed in Fig. 1a and b cannot be quantitatively compared because the recorded signal depends on numerous experimental factors. Each Raman spectrum has been independently scaled for clarity in both figures.

Fig. 1b shows the Raman spectra of sample B with Cu–Ag core-shell nanoparticles at different energies. The spectra present two different Raman peaks in contrast to those of Fig. 1a. Only one peak associated with the quadripolar mode is expected. The additional peak might be attributed to radial mode or to an another nanoparticle specie. The intensity of the radial mode is generally weaker than that of the quadripolar mode and can only be observed with a narrow size distribution of particles. The unexpected nanoparticle specie is suspected to be at the origin of the new Raman peak. To determine this origin, TEM images has been performed using EFTEM and HRTEM techniques. The EFTEM image of Fig. 2c shows the Cu–Ag core shell structure of the nanoparticles. The contrast is obtained by the image reconstruction exclusively with the electrons that have lost characteristic energy by inelastic interactions with silver. One extra nanoparticle specie is also visible: small white dots which may be interpreted as pure Ag nanoparticles or core-shell nanostructures beyond the spatial resolution of EFTEM images. HRTEM analysis has been done on these small particles. The crystallographic analysis of the lattice fringes corresponds to pure Ag nanoparticules. These latters are formed due to the Ag atoms that cannot escape from local energy minima imposed by the available nucleation sites on the amorphous carbon film. From these observations, we have calculated the diameter of the both particle species from the frequency of the Raman peaks. Eq. (1) is directly used to compute the vibration frequencies of pure Ag particles. The deduced Ag particle diameter for an excitation at 2.7 eV is reported in Table 1 in agreement with the mean
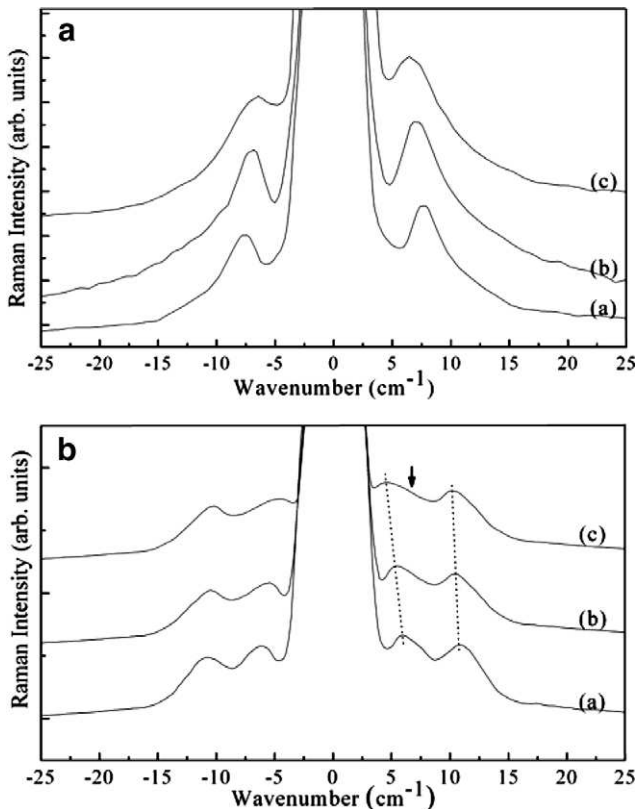


Fig. 1. Low frequency Raman spectra of (a) Cu nanoparticles and (b) Cu–Ag core-shell nanoparticles excited at (a) 2.7 eV, (b) 2.41 eV, (c) 1.65 eV. The small observed peaks observed from each parts of the Rayleigh ($0 \, cm^{-1}$) are associated with quadripolar vibrations.
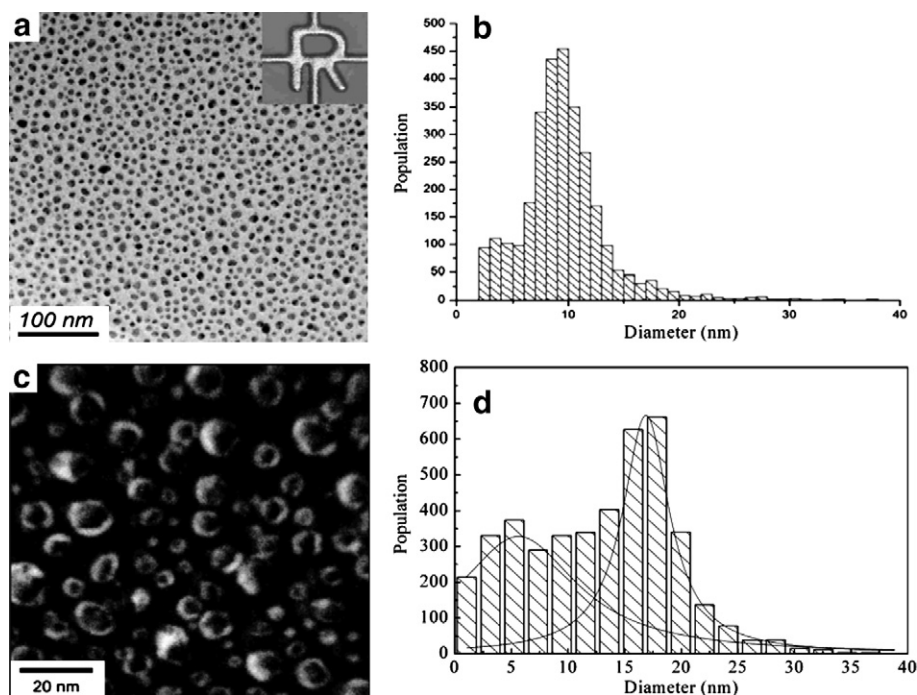
Fig. 2. (a) Bright field TEM image of nanoparticles (sample A) on the area formed by the letter R of the numeration items and the rods of the microscopy grid [see inset], (b) diameter distribution of Cu nanoparticles, (c) EFTEM images of Cu–Ag core-shell nanoparticles (sample B), (d) distribution of Cu–Ag nanoparticles (the full line is the Lorentzian fit).

Table 1
Nanoparticle sizes (nm) measured by micro Raman and TEM on Cu, Cu–Ag and Ag nanoparticles

|  | Cu | Ag shell | Ag |
|---|---|---|---|
| Micro Raman | 9 | 1.6 | 4.6 |
| TEM | 9.6 | 1.8 | 5.4 |

diameter measured by TEM. The quadripolar modes of Cu–Ag core-shell nanoparticles can be calculated with the Lamb's approach including the Navier equation. Further, we used the mean diameter deduced from the Cu nanoparticles of sample A as the core diameter to calculate the Ag shell thickness (Table 1). The values are in agreement with the TEM measurements. One can notice that the lower frequency peak shifts towards the Rayleigh line from 5.8 to 4.9 $cm^{-1}$ with decreasing the excitation energy. The shift of the upper peak between the extreme wavelengths is quite constant with a value of only 0.4 $cm^{-1}$. The both behaviours are the same as the one witnessed in Cu nanoparticles and are due to the excitation of the nanoparticle with a form that tends to an ellipsoidal shape shifting the excitation to the red. The values of these shifts indicate that the Ag nanoparticles have a more spherical shape than the Cu–Ag nanoparticles.

It has been shown that the intensity of the Raman peak associated with nanoparticles is proportional to the inverse size distribution. Up to now, Raman scattering on nanoparticles has been limited to macroscopic scale avoiding the direct comparison between the nanoparticle size distribution obtained by TEM and the Raman intensity [14]. The reduction of the Raman probe to a μ scale allows this

comparison. Fig. 2(d) exhibits the two components related to Cu–Ag and Ag nanoparticles in the diameter distribution obtained with HAADF images on sample B. Fig. 3a
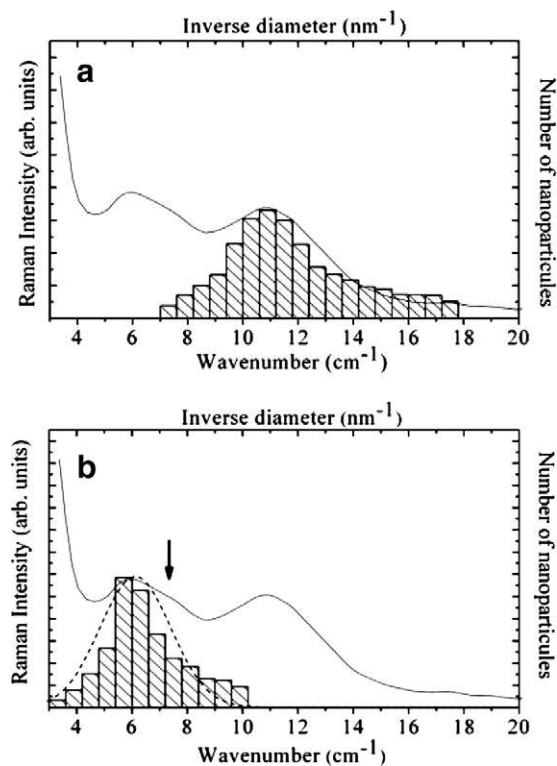


Fig. 3. Superpositions of the Stokes Raman spectrum [Fig. 1(b)] recorded at 2.7 eV on the inverse diameter distribution for (a) Ag and (b) Cu–Ag core-shell nanoparticles (the dashed line is a Gaussian fit on the maximum of the Raman peak).
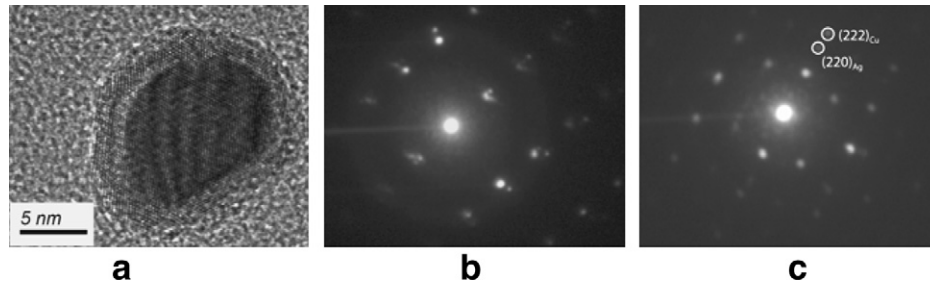
Fig. 4. (a) High resolution images showing lattice fringes of the Cu core and the surrounding Ag shell (b) and (c) diffraction patterns (nanobeam mode, probe size 1 nm) on two single core-shell nanoparticles in zone axis. Perfect epitaxy relationship is evidenced inn (b) by two corresponding $(2\bar{1}1)$ zone axis. A second epitaxy relationship is revealed in (c), with a $(2\bar{1}1)$ zone axis for Cu and a $(100)$ zone axis for Ag.

and b shows the Raman spectrum of sample B (measured at 2.7 eV) superimposed with the inverse diameter distribution deduced from TEM of Ag and core-shell Cu–Ag nanoparticles, respectively. The Raman intensity of Ag nanoparticles is in good agreement with the inverse diameter distribution. A discrepancy appears in Fig 3b for the Cu–Ag nanoparticle around 7–8 cm$^{-1}$. The Raman intensity decreases slowly compared with the inverse diameter distribution. This can be seen more clearly in the spectrum of Fig. 1b recorded at a lower energy. On one hand, compared to Ni–Ag core-shell particles where only the Ag shell vibrations has been observed [13], the presence in the Raman spectra of sample B of a peak associated with Cu–Ag core-shell nanoparticles indicates the good phase matching of the acoustic wave between the shell and the core. The bonding seems thus to be stronger between Ag and Cu than between Ag and Ni. On the other hand, the discrepancy is located at the same wave number as the Cu nanoparticle peak of Fig. 1a. The additional contribution can originate from Cu–Ag nanoparticles with a weak bonding between Ag and Cu atoms leading to a Raman signal from the free Cu core and Ag shell. The latter is hidden in the high wave number signal. As Raman and TEM measurements have been performed on the same micron area, the Raman interpretation can be correlated with TEM observations. Fig. 4 presents the diffraction acquired in nanobeam mode on a single nanoparticle. It clearly shows that there are at least two different epitaxy relationships between the Cu core and the Ag shell. The first one is a perfect epitaxy, which means that Ag adopts exactly the subjacent structure of Cu. The two crystallographic orientations are then rigorously the same. This is pointed out in Fig. 4b by a $[2\bar{1}1]$ zone axis for the two crystals, and a perfect matching between equivalent directions. The second epitaxy relationship is visible in Fig. 4c. On this nanodiffraction image, the indexing of the diffraction pattern informs us about the respective zone axis of silver and copper. Copper crystal is oriented along a $[2\bar{1}1]$ zone axis, whereas the surrounding silver crystal presents a $[100]$ zone axis perpendicular to the electron beam. The directions $[1\bar{1}1]$ for Cu and $[2\bar{2}0]$ for Ag are parallel in the plane of the figure. The different orientations between the crystallographic axes of Cu core and Ag shell reduce the sound phase matching between atoms and induce the additional contribution in the Raman spectra of free Cu core.

## 5. Conclusion

The reduction of the Raman probe area allows us to directly compare the nanoparticle sizes, form and composition deduced from the quadripolar mode to the ones obtained from TEM images. The confined vibration modes related to Cu–Ag core-shell and pure Ag nanoparticles have been identified in the same spectrum. Two components in the Raman spectra, depending on the acoustic mismatch between Cu core and Ag shell have been discerned and correlated with their respective crystallographic orientations measured by nanodiffraction.

## References

[1] M. Moskovits, Rev. Mod. Phys. 57 (1985) 783.
[2] J.I. Gersten, A. Nitzan, Surf. Sci. 158 (1985) 165.
[3] D.A. Weitz, T.J. Gramila, A.Z. Genack, J.I. Gersten, Phys. Rev. Lett. 45 (1980) 355.
[4] H. Portales, L. Saviot, E. Duval, M. Fujii, S. Hayashi, N. Del Fatti, F. Vallee, J. Chem. Phys. 115 (2001) 3444.
[5] E. Duval, A. Boukenter, B. Champagnon, Phys. Rev. Lett. 56 (1986) 2052.
[6] M. Fujii, T. Nagareda, S. Hayashi, K. Yamamoto, Phys. Rev. B 44 (1991) 6243.
[7] B. Palpant, H. Portales, L. Saviot, J. Lermé, B. Prével, M. Pellarin, E. Duval, A. Perez, M. Broyer, Phys. Rev. B 60 (1999) 17107.
[8] W. Grogger, M. Varela, R. Ristau, B. Shaffer, F. Hofer, K.M. Krishnan, J. Electron Microsc. 143 (2005) 139.
[9] C. Ricolleau, L. Audinet, M. Gandais, T. Gacoin, Thin Solid Films 336 (1998) 213.
[10] G. Bachelier, A. Mlayah, Phys. Rev. B 69 (2004) 205408.
[11] L. Saviot, D.B. Murray, Phys. Rev. B 72 (2005) 205433.
[12] H. Lamb, Proc. Math. Soc. Lond. 13 (1882) 187.
[13] H. Portales, L. Saviot, E. Duval, M. Gaudry, E. Cottancin, M. Pellarin, J. Lermé, M. Broyer, Phys. Rev. B 65 (2002) 165422.
[14] E. Duval, H. Portales, L. Saviot, M. Fujii, K. Sumitomo, S. Hayashi, Phys. Rev. B 63 (2001) 75405.